Relative influence of surface topography and surface chemistry on cell response to bone implant materials. Part 1: Physico-chemical effects

A Ponche, M Bigerelle, K Anselme

Relative influence of surface topography and surface chemistry on cell response to bone implant materials. Part 1: Physico-chemical effects

A Ponche[1], **M Bigerelle**[2], and **K Anselme**[1]*
[1]Institut de Sciences des Matériaux de Mulhouse (IS2M), CNRS LRC7228, Université de Haute-Alsace, Mulhouse, France
[2]Laboratoire Roberval, CNRS UMR6253, Centre de Recherche de Royallieu, Université de Technologie de Compiègne, Compiègne, France

Abstract: Knowledge of the complexity of cell–material interactions is essential for the future of biomaterials and tissue engineering, but we are still far from achieving a clear understanding, as illustrated in this review. Many factors of the cellular or the material aspect influence these interactions and must be controlled systematically during experiments. On the material side, it is essential to illustrate surface topography by parameters describing the roughness amplitude as well as the roughness organization, and at the scales pertinent for the cell response, i.e. from the nano-scale to the micro-scale. Authors interested in this field must be careful to develop surfaces or methods systematically, allowing perfect control of the relative influences of surface topography and surface chemistry.

Keywords: surface topography, surface chemistry, roughness measurement, roughness parameters, implant, bone, coatings, surface treatments, XPS

1 INTRODUCTION

Metallic hip prostheses and dental implants have been used successfully for several decades in orthopaedics and dental surgery. However, non-integration of the implants in surrounding bone tissue is sometimes observed without any evident cause. The understanding of how cells and tissue interact with the implant surface is then needed, with the aim to optimize implant surface performance. For several years, the current authors and others have tried to describe and understand the mechanisms under the human bone cell response to materials used in orthopaedics and dental surgery for bone filling or bone replacement [**1**–**5**]. This review, divided into two companion papers, is intended to give an overview of the most important mechanisms underlying the cell response to a material's surface. The physico-chemical aspects will be described in this first part and the biological aspects in the second part. To cover these different aspects, the review was written together with a material scientist, a physico-chemist, and a biologist, all specialists of the interfaces of materials with biological elements.

Surface features like topography and chemistry are known to be influencing factors for cells. However, the distinction between their relative effects is extremely difficult to achieve on implant materials because of the complexity of their composition and the process used for changing their topography or chemistry. Indeed, it is almost impossible to modify surface topography of implant materials without changing surface chemistry at the same time [**6**]. One possibility to overcome this difficulty is to process model materials, i.e. materials with homogenous composition (not alloyed), and use a process that does not apply energy that is too strong. The approaches based, for example, on nano- and micro-patterning are effectively very useful for understanding the mechanisms of cell response to topography, but they produce surface morphology and surface chemistry very different from what is observed on a real implant surface. Another possibility to discriminate the relative influence of topography and chemis-

**Corresponding author: UHA, Institut de Science des Materiaux de Mulhouse, 15 rue jean starcky, BP2488, Mulhouse, 68057, France.*
email: karine.anselme@uha.fr

try is to cover the surface with a thin layer of another material in order to control the surface chemistry, but without changing the surface topography (at least at the micrometre scale) [**7**–**10**]. To make a replica of the surface in another material is another alternative [**11**, **12**].

An important point in the characterization of surface topography is the definition of the pertinent parameters that can be identified in relation to the cellular response. Very frequently, the parameters used for describing surfaces or cell response are too limited in number and in relevance. Notably, the parameters describing roughness amplitude are generally privileged, although the parameters describing surface morphology and organization have been shown to have a better pertinence to human bone cell adhesion [**13**]. Additionally, surface and biological parameters are very rarely correlated together. In this first paper, the benefits of using a statistical approach to determine the best pertinent surface parameters for describing the biological response will be illustrated. Other important parameters need to be considered in these studies, such as the scale of analysis. The surface topography must be analysed not only at the cell scale but also at the scale below the cell scale, because, as will be described in this review, the mechanisms underlying cell response to the surface pass through proteins adsorbed on surfaces, cell membrane receptors and cytoskeleton molecules, all of them being at the nanometre scale.

The surface chemistry must also be perfectly controlled and characterized beforehand to study cell behaviour since, as seen previously, the modification of surface topography will modify concomitantly the surface chemistry. Various techniques exist to characterize surface chemistry and these will be described briefly here. The importance of preparation treatments for implants will be highlighted in particular.

The cellular mechanisms involved in cell–surface interactions will be described in the companion paper of this review.

2 DEFINITION OF SURFACE TOPOGRAPHY

The objective of this section is to establish basic and essential notions in roughness measurement and analysis to allow the reader to proceed correctly with roughness characterization before correlating these measurements with parameters describing functionality such as the biological functions (cell adhesion, migration, proliferation, etc.). First, the different apparatus that can be used will be described, focusing notably on the respective advantages and disadvantages. Second, the basic notions under roughness measurements will be defined, such as scale and resolution notions. The respective interests and limits of two-dimensional (2D) or three-dimensional (3D) measurements will be discussed. Finally, the notion of multiscale analysis will be introduced before the description of global analysis systems that allow definition of the best pertinent roughness parameter and its relevant scale for describing a specific functionality.

2.1 Apparatus

There are principally three types of roughness measurement apparatus: stylus profilometer, atomic force microscopy (AFM), and optical apparatus. In this part, the focus is solely on the advantages and disadvantages of these techniques [**14**–**16**].

2.1.1 Atomic force microscopy

For topographical investigations, the major limitation of AFM is that the response of the piezo scanner to voltage is not linear [**17**]. This leads to hysteresis, bow, drift, creep, and cross-coupling in the displacement of the piezo and errors in the displacement measurement, especially for large displacement [**18**]. The use of displacement sensors and servo loop system is useful to limit this problem, especially when accurate measurements are needed, but tends to add noise on the topographic signal. At the nanometre scale, the resolution of the image is limited by the non-vanishing size of the probe. Even if atomic resolution could be achieved, in most cases the tip is not sharp enough to describe the surface features correctly. The AFM image is the result of the interaction between the tip and the sample surface. This phenomenon known as dilation tends to smooth the sharp features and fill the holes [**19**]. Nevertheless, AFM offers an incomparable resolution and is the ideal tool to describe topography at the submicrometre scale.

2.1.2 Stylus profilometry

The principal advantages of this technique [**20**] is that the stylus is in contact with the surface and consequently the contact gives the amplitude level of the roughness with good accuracy and without depending on the optical properties of the surface. Another advantage is that this class of roughness recorder can measure a wide range of roughness amplitudes from 10 nm to over 1 mm. However, this apparatus also possesses several disadvantages. As the method is

based on contact, a force is applied on the surface by the stylus and this can damage the surface by plastic deformation. Moreover, on substrates with a low rigidity, elastic deformation can disturb the measurement. Another artifact, also encountered with AFM, is that the tip radius of the stylus [50 nm–10 μm] will smooth the surface and does not allow the more deep and narrow valleys to be recorded [**21**, **22**]. Finally, the relatively high speed of the stylus can cause it to jump over peak roughness, which can change the peak curvature [**23**]. However, all theses artifacts can be easily quantified (scanning electron microscopy (SEM) observation of the surface, tip radius simulation algorithms, etc.). It should be noted that 3D measurement can be made using a tactile profilometer, but this is a very long process since it is basically composed of a succession of 2D measurements with a y displacement given by a motor table that can induce a lower definition in the y direction.

2.1.3 Optical profilometry

Several optical techniques have been developed to record surfaces [**24**]. Rather than describing each technique, their common advantages and disadvantages will be summarized. The major advantage is that there is no contact with the surface, suppressing all risk of defects induced by contact mechanics. Such apparatus gives principally 3D measurements and possesses the same resolution in both directions. The time measurement is much reduced compared with AFM and stylus profilometry. The major disadvantage of this technique is that the measurement is very sensitive to both the optical surface properties and the surface topography. Contrary to contact measurement, the artifacts introduced by this apparatus are very difficult to quantify. For example, if the slope of the roughness is too high, then measurements cannot be processed. If a roughness step exists around the wavelength, an artificial peak can be created (known as the 'batwings effect') [**16**]. A second disadvantage of these techniques is that their resolution is low and limited around 1000 data by direction, and that is a very poor definition. Some stitching techniques (the process of combining multiple elementary topographical maps with overlapping fields of roughness to produce a high-resolution topographical map) exist to increase this resolution, but they drastically increase time of acquisition and introduce a high number of artifacts during surface reconstruction. The last disadvantage is that results depend on both the microscope objectives and the filter used in the signal treatment, which depends greatly on the apparatus itself.

As shown shortly, the choice of apparatus to measure roughness is a very difficult task. Moreover, the comparison of roughness measured with different apparatus such as AFM, optical and tactile profilometer is hardly possible even if the roughness is evaluated at the same scale. Differences in roughness amplitudes between different apparatus can be higher than the differences that characterize the different surfaces.

2.2 Particular properties of surface roughness

Before analysing the roughness measurements, the surface has to be recorded. Whatever the roughness measurement, the roughness term means that the surface amplitude defined by z is given by a function of $z=f(x)$ for a profile recording and $z=f(x,y)$ for a surface recording. The first important remark is that it is impossible for any apparatus used for surface topography characterization to record surface when the roughness is composed of caverns, or more precisely when $z=f(x,y)$ is not unique for a fixed (x,y). Actually, all apparatus give the value of $z=Sup[f(x,y)]$. In reality, a high number of surfaces used in the biomaterial field do not possess caverns, such as machined surfaces treated by grinding, cutting, sandblasting, etc. However, some can possess this structure, such as porous materials, some sputtered films, and so on (Fig. 1). Yet there is no protocol in the ISO roughness normalization to verify this assumption. At the usual scale of observation met in the literature (μm), no non-destructive techniques exist that can be used to verify that no caverns are present on the surface topography. The only available techniques are destructive and consist of cutting the surface orthogonally by high-precision cutting techniques (laser, water jet, focused ion beam (FIB), etc.) and observing the resulting sections microscopically.

2.3 The pretreatment of profiles

After measurement, a recorded profile $r(x,y)$ is obtained. The main problem is that in all apparatus measurements, the values of $r(x,y)$ are given at an origin that is external to the surface and cannot be determined. The following step consists of finding an origin to the surface. This step is of major interest and is still subject to controversy. Roughly speaking, a smooth function $s(x,y)$ is chosen and considered as the zero-level elevation surface. The basic idea is that the mathematical expression of this function is chosen so that roughness is not modified. For example, if

Fig. 1 Example of limited aggregation structure simulated by a ballistic model presenting porous structure. The upper line (black) represents $z = Sup[f(x,y)]$, which will be the measured roughness

roughness is measured on the femoral head of a hip prosthesis, then the form represents a circular shape on which roughness is present (scratches, cutting roughness, and so on). At the scale of the prosthesis, a third degree polynomial form can be used to approach $s(x,y)$ [**25**, **26**]. Then a final profile z is obtained such as $z(x,y) = r(x,y) - s(x,y)$. How to affirm that $s(x,y)$ is the appropriate form? Answering this question is not a simple task. $s(x,y)$ is well adapted if and only if

(a) $z(x,y)$ becomes stationary, i.e. roughness parameters computed from the surface do not statistically change after a characteristic length that is lower than the evaluation length L (around $L/5$).
(b) $s(x,y)$ does not contain any topographical information of the ideal surface $z^{\text{ideal}}(x,y)$.

The first condition is easy to verify with classical signal processing operators (such as autocorrelation length). The second one is impossible to verify by an automatic procedure because $z^{\text{ideal}}(x,y)$ is unknown. This point is of major interest in the field of surface roughness characterization and must be specified in published results because, in the current authors' opinion, roughness measurements cannot be compared in the literature of the biomaterials field without this information.

Suppose that $s(x,y)$ contains information that is related to the surface functionality. Then this information is lost and can no longer be related to biological properties. For example, suppose that cell adhesion depends on a wave on the surface and that this wave is included in $s(x,y)$. Then, no correlation can be found between this form and cell adhesion [**27**]. More drastically, it is possible to filter surface roughness (low pass filter, high pass filter) that in fact leads to a new function $s'(x,y)$ such as $z(x,y) = r(x,y) - s(x,y) - s'(x,y)$. Thus, the value of $s'(x,y)$ can also remove biologically relevant information. This clearly means that the choice of $s(x,y)$ and/or $s'(x,y)$ must be considered with respect to function of the biological properties analysed in the biomaterials.

2.4 The scale and resolution of measurements

One important aspect in surface measurements is to choose the scale at which measurements must be carried out [**28**, **29**]. Let $Z(x,y)$ denote the original surface: the measure of the surface is often a subsurface $z(x,y) \subset Z(x,y)$ that is discretized into a grid $z(i\Delta x, j\Delta y)$ for $i \in \{1, \ldots, N_x\}$ and $i \in \{1, \ldots, N_y\}$. This is very important because for a lot of roughness apparatus (confocal microscope, AFM, interferometer) the number of N_x and N_y is fixed (lying between 256 and 2048, and more often around 500). As claimed previously, the roughness must be stationary at the scale $(N_x\Delta x)/5$ and $(N_y\Delta y)/5$, meaning that the information lying between $[\Delta x, (N_x\Delta x)/5]$ must lie in about 100 discretized points. This lead to the following important remarks.

1. The choice of Δx (the sampling length), which is imposed by the magnification, governs the observation scale.
2. From the Shannon theorem $\Delta x > \delta/2$, where δ is the smallest detail required for analysis, the resolution of 100 points is reduced to 50 points. More drastically, for fractal surfaces, the Shannon theorem fails and can lead to $\Delta x > \delta/10$.

This means that for each apparatus, the scale on which the phenomenon is governed must be perfectly known. The stitching method is a palliative solution, but this technique introduces several artifacts that will not be discussed in this paper. As a consequence, in all roughness study, the scale on which measurements must be made requires a great deal of attention and governs all conclusions. These points will be discussed in the next section.

2.5 Two- or three-dimensional roughness measurements

According to the measurement system, 3D or 2D measurements can be taken, meaning that a profile

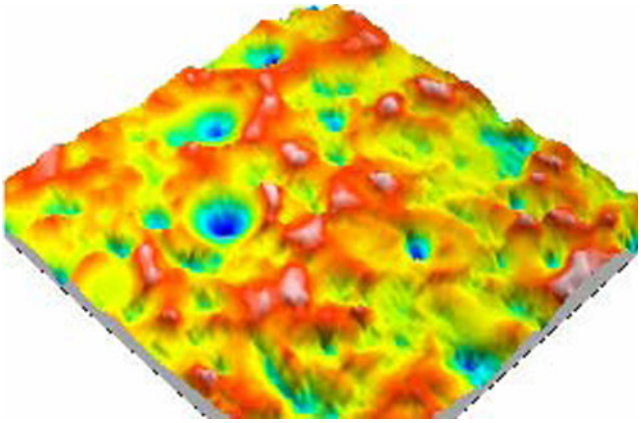

Fig. 2 Examples of an isotropic titanium surface obtained by electro-erosion

or a surface respectively is recorded. In rough terms, a 2D measurement contains a high number of points (often $>10\,000$), whereas in 3D measurement the resolution, as shown previously, is very low (around 256–1024 points in a given axis direction). On the contrary, 3D measurements allow the surface to be seen and in all the directions. A surface can be considered as isotropic if its roughness is similar in all directions and more precisely if all profiles extracted from the surface, whatever the direction, lead statistically to the same profile, i.e. give statistically the same value of roughness parameters (Fig. 2). In this case, it can be admitted that 3D measurements do not introduce more information than 2D measurements. On the contrary, if a surface is anisotropic, then the roughness depends on the direction, and roughness values must be used in specifying the direction of evaluation. In a high number of topographic surfaces, the directions of anisotropy are orthogonal and can be decomposed into two principal directions. Then their treatment can be carried out only in these two directions (Fig. 3). This point is of major interest since it can be easily understood; taking only one roughness parameter does not allow the anisotropy of the surface to be taken into account. A single parameter will average the two directions. Thus, at this stage, it would be more appropriate to decompose surfaces in profiles in the principal directions and to compute roughness parameters from the profiles. However, in 2D measurements, an artifact can appear that is not clearly mentioned in the literature. For example, in 2D measurements, the norm refers to 'peaks and valleys' to describe topography. However, when high peak amplitude is recorded in two dimensions, it is not really the highest altitude of the real peak visible in three dimensions. Indeed, the 2D peak amplitude will be always lower than the real 3D amplitude. It will only be equal if the profile scan passes exactly through the maximum of the 3D peak and that has a very low probability in a statistical sense. Unfortunately, no generic method exists to correct two dimensions.

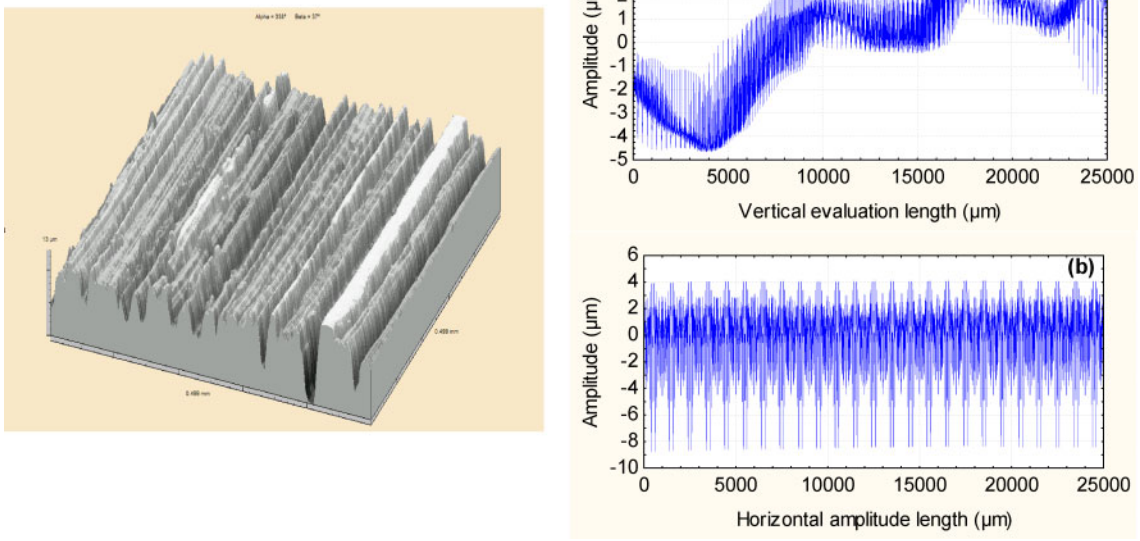

Fig. 3 Three-dimensional measurement of an explanted knee prosthesis in CrCo after abnormal wear. (a) Two-dimensional profile in the wear direction (vertical, i.e. in the y direction). (b) Two-dimensional profile perpendicular to the wear direction (horizontal, i.e. in the x direction)

2.6 The roughness parameters

Basically, surface roughness 2D parameters are normally categorized into three groups according to their functionality [**30**]. They are defined as amplitude parameters, spacing parameters, and hybrid parameters. These definitions are the same in three dimensions, but another category appears that is spatial parameters such as, for example the density of summits, the texture direction, or the dominating wavelength [**31**]. The most used roughness parameter in the biomaterials field is the well-known R_a parameter [**32**, **33**].

$$Ra = \frac{1}{N}\sum_{i=1}^{N} |z_i| \tag{1}$$

Another interesting parameter is S_m, which represents the average peak number on the profile.

Consider the scheme of four simulated surfaces obtained by the same process with different machining parameters (Fig. 4). Surfaces (A, C) have the same R_a and the same is true for surfaces (B, D). On the contrary, surfaces (C, D) like surfaces (A, B) have the same S_m. This clearly means two things [**34**]

(a) R_a is unable to characterize lateral roughness;
(b) one parameter is not enough in this case to characterize the surface.

More importantly, the R_a is unable to see the skewness of the profile, i.e. it cannot distinguish peaks and valleys. Then some amplitude parameters such as the skewness (Sk) must be used to see this difference [**35**].

2.7 The multiscale measurements

As shown previously, the value of a roughness parameter can depend on the scale of measurement. The concept of multiscale analysis will now be introduced. Consider a macroscopic profile (Fig. 5). Considering a scale ε that defines a window, a second rectification can be performed by a polynomial fitting. Then, roughness parameters are calculated on the resulting profile, defining values of these parameters at the scale ε. This method is equivalent to the filtering of high wavelengths that allow the micro-roughness to become apparent.

The calculation of roughness parameter values can then be applied on each profile obtained at different evaluation lengths. For example, the $R_a(\varepsilon)$ is obtained, meaning that the R_a depends on the scale ε. In fact, all roughness parameters can then be computed at different scales [**36–39**]. The major interest of the multiscale analysis is then to find the optimal scale that describes best the surface functionality and this will be the basis of the next section.

2.8 The choice of a roughness parameter and its relevant scale

There is increasing interest in developing reliable methodologies suitable for quality control stage processes for the surfaces of products in a manufacturing environment. The various industrial and scientific interests in topography analysis mean that a proliferation of roughness parameters, possibly running into hundreds, has been triggered to describe the different kinds of surface morphology with regard to specific functions, properties or applications. In spite of this

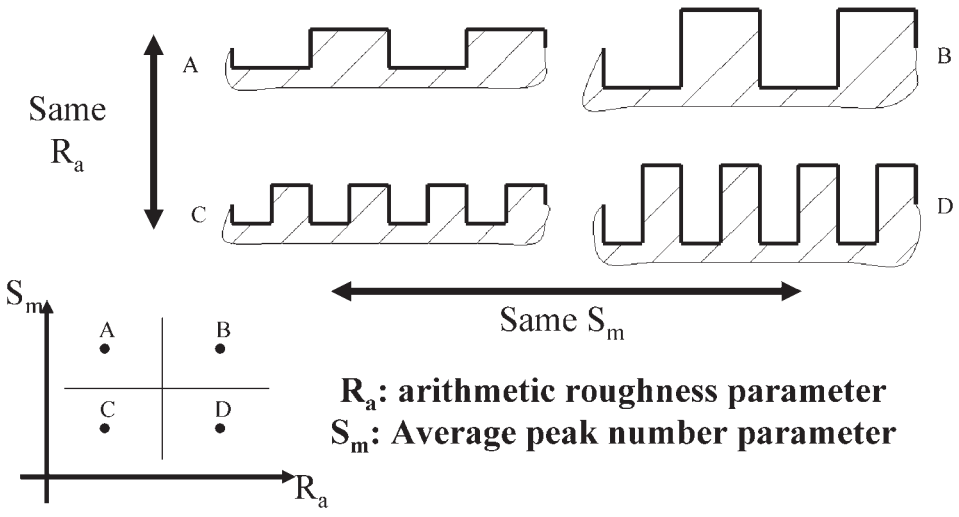

Fig. 4 Example of profiles both giving the same R_a $(A = C) \neq (B = D)$ and S_m parameter $(A = B) \neq (C = D)$

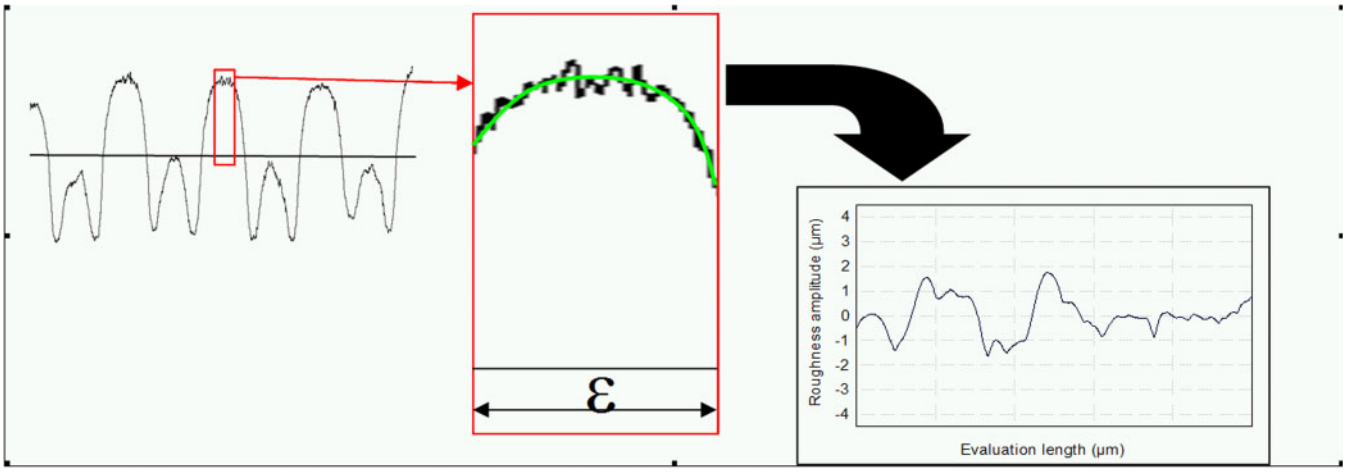

Fig. 5 Principle of a multiscale analysis. An original profile is recorded (left) and a scale function (centre) is defined on a window ε from which the original profile is subtracted to obtain a new profile (right)

proliferation, termed by Whitehouse the 'parameter rash', there is still no complete understanding of the relevance of these roughness parameters. This probably comes from a lack of global methodology combined with the limits of the software presently on the market whose function is to characterize a surface morphology. In the present authors' opinion, the main objective of such a global methodology must be to determine quantitatively, and without preconception, the most relevant roughness parameter that can characterize the surface morphology of a manufactured product with regard to a particular function, property or application. Then the question that arises is: 'which parameter is the most relevant one to characterize the morphology of a machined surface with regard to a specific application, such as cell adhesion for example?' The main purpose is to answer the previous question without any preconceived opinion on the surface roughness parameters and the scale at which they must be evaluated [**40**].

With the objective to answer this question, an original surface analysis system called 'MesRug' has been designed [**41**–**44**]. The interest of this system is to build a robust statistical analysis to create a probabilistic index, independent of the number of parameters that characterize the relevance of each roughness parameter. For this reason, a recent data analysis tool called the 'bootstrap' is used. This technique allows the process conditions to be found that give the best correlation with a physical or a biological process [**41**].

The importance of this approach will be illustrated through the correlation of wettability and surface roughness of titanium surfaces. The basic question is: 'does the roughness of a surface influence its wettability?' when the surface chemistry has been described as homogeneous after verification by XPS. Thirty surfaces were tooled by electro-erosion process to obtain a high range of roughness amplitudes. First, it is supposed that if a relation exists between surface roughness and wettability, an analytical form of this relation could be formulated. In a first attempt, a linear relation such as: $\theta(\varepsilon) = \alpha(\varepsilon) \times \text{Roughness}(\varepsilon) + \beta(\varepsilon)$ is retained. When θ is the contact angle, ε is the scale of relevance, $\text{Roughness}(\varepsilon)$ is a roughness parameter evaluated at the scale ε, and (α, β) are two parameters obtained by the least-squares method that represent the relation between roughness parameter $\text{Roughness}(\varepsilon)$ and wettability θ.

Second, a multiscale treatment of the surface is processed. Figure 6 illustrates the original profile analysed at two different scales of observation: 63 and 210 µm. Then, for all surfaces and at all scales, roughness parameters are computed (more than 100). To illustrate the methodology, only the R_a will be presented. For this purpose 30 profiles are recorded for the 30 surfaces (indiced by k) and ten angle measurements are processed on each surface. Then to quantify the variation in both of these measures (i.e. angle θ and roughness parameter $\text{Roughness}(\varepsilon)$), the bootstrap is used: for each pair k corresponding to the k^{th} ($k \leqslant 30$) of the 30 surfaces, 30 values of $R_a(\varepsilon, k)$ are taken randomly for each k surfaces with replacement and ten measures of angle measurements $\theta(k)$ are also taken randomly. Then both means $\left(\bar{R}_a(\varepsilon, k), \bar{\theta}(k)\right)$ are computed. This is a first bootstrap simulation noted $\left(\bar{R}_a^1(\varepsilon, k), \bar{\theta}^1(k)\right)$. This step is then reproduced p times to obtain a set of

bootstrap sample $[(\bar{R}_a^1(\varepsilon,k),\bar{\theta}^1(k)),(\bar{R}_a^2(\varepsilon,k),\bar{\theta}^2(k)),\ldots,(\bar{R}_a^p(\varepsilon,k),\bar{\theta}^p(k))]$. Figure 7 represents 100 bootstrap samples for the 30 surfaces. For each i bootstrap samples $\{(\bar{R}_a^i(\varepsilon,1),\bar{\theta}^i(1)),(\bar{R}_a^i(\varepsilon,2),\bar{\theta}^i(2)),\ldots,(\bar{R}_a^i(\varepsilon,30),\bar{\theta}^i(30))\}$, the values of (α,β) noted (α^i,β^i) can be computed, thanks to the least-squares method. The classical critical value $p_c(R_a(\varepsilon))$ noted $p_c^i((R_a(\varepsilon)))$ that represents, under the Gauss Markov hypothesis, the probability to reject wrongly the fact that $\alpha(R_a(\varepsilon))=0$, is computed. The lower is $p_c(R_a(\varepsilon))$, the higher is the correlation between $R_a(\varepsilon)$ and contact angle θ. It is then possible to plot all different $p_c(R_a(\varepsilon))$ values of bootstrap samples versus evaluation length as shown on Fig. 8. By analysing all the scales, it is shown that the best relation is obtained if this $R_a(\varepsilon)$ is computed at the scale of 210 µm, i.e. $R_a(210\ \mu m)$. As it can be effectively observed on Fig. 7(b), a very nice linear relation is found between R_a and contact angle at this scale. Otherwise, when the topography $R_a(\varepsilon)$ is evaluated at the scale of 63 µm, i.e. $R_a(63\ \mu m)$ (a classical evaluation length for AFM), the linear relation will not be any more clearly shown (Fig. 7(a)). Then, the methodology proposed here (and developed in the present authors' software Mesrug) makes it possible to demonstrate that the R_a is the best parameter, i.e. no other parameter exhibits a better correlation (result not shown) to characterize the wettability, but only if this one is evaluated at the scale of 210 µm.

Finally, this illustrates that roughness characterization must always be carried out at the best relevant scale according to the functionality analysed.

To conclude this section, different notions must be kept in mind before measuring and treating surface topography. First, the reader must be conscious that the choice of the apparatus for measuring roughness will have a strong influence on the outcome and should be adapted to the surface measured or to the objectives addressed. Second, the pretreatment applied on measured profiles must be adapted to the required functionality of the surface, since these pretreatments could remove relevant information from the profiles. Third, the reader is informed that surfaces cannot generally be characterized by only one roughness parameter and that the association of amplitude, spacing, and hybrid parameters must be preferred. Finally, it has been shown that a multiscale analysis and the use of expert systems are preferable to determine the best discriminate scale of analysis and the best roughness parameter for analysing a specific functionality.

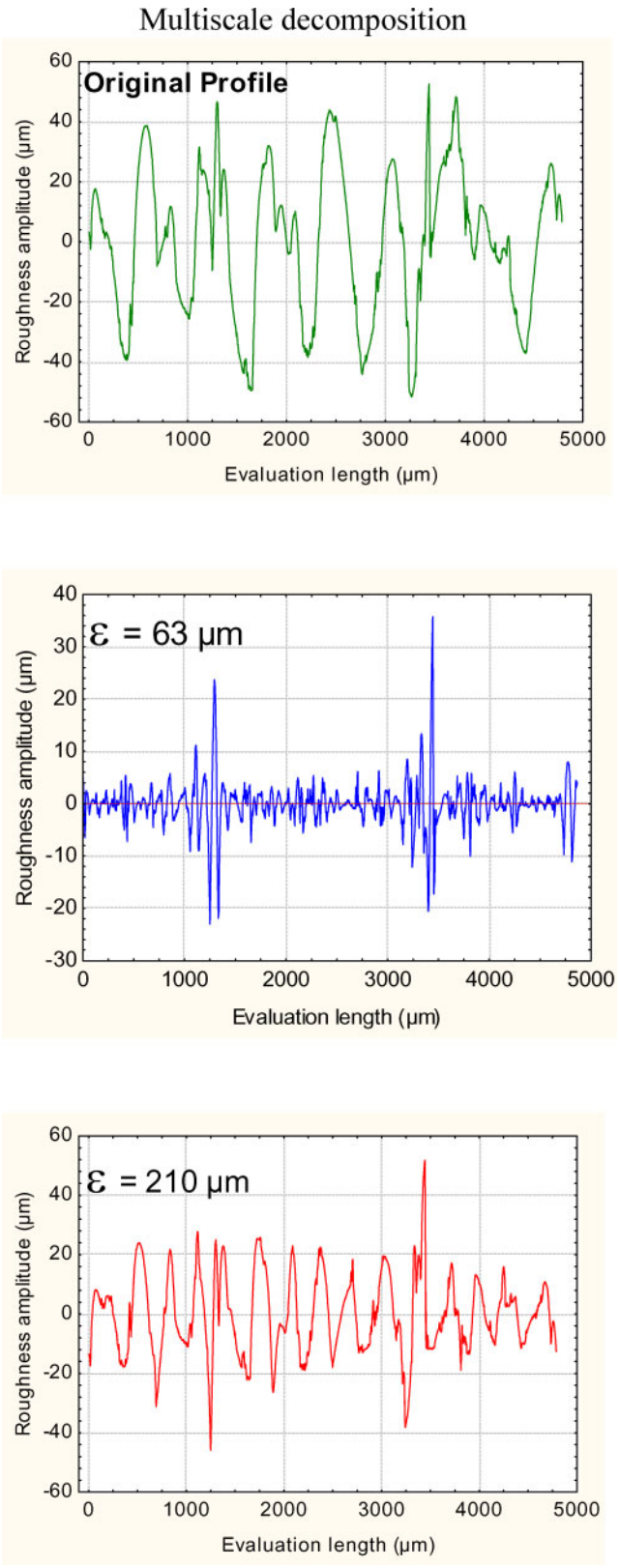

Fig. 6 Multiscale analysis of a titanium electro-eroded surface: two multiscale profiles evaluated at the scale $\varepsilon = 63\ \mu m$ and $\varepsilon = 210\ \mu m$

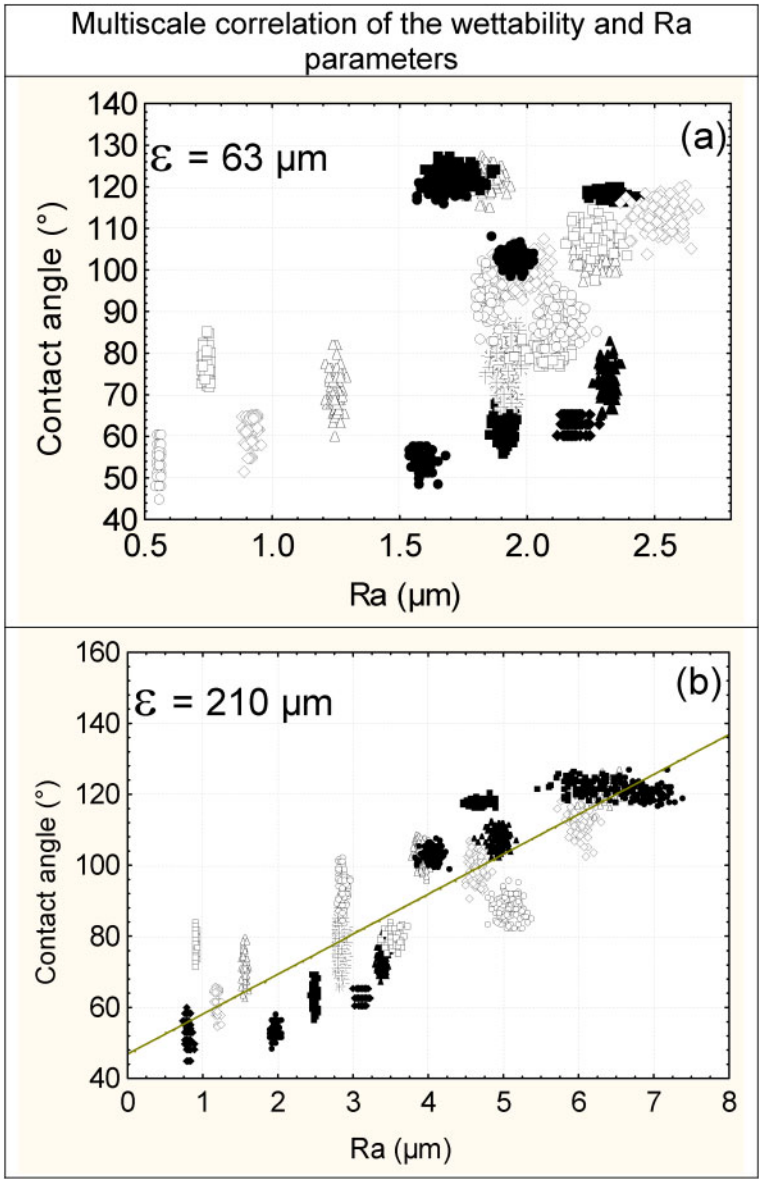

Fig. 7 Relationship between the contact angle and the R_a evaluated at the scale $\varepsilon = 63\,\mu m$ and $\varepsilon = 210\,\mu m$ (computed from the profile shown in Fig. 6)

3 DEFINITION OF SURFACE CHEMISTRY

Performances of implanted materials are intrinsically linked to interactions between biological fluid and surface of the implants. This interaction is often mediated by proteins adsorbed from the biological fluid. Characteristics of the surface in term of roughness, topography, and surface chemistry are then transcribed by the protein layer in information that is comprehensible for the cells [**1**].

3.1 Process

The increase of performance of implants upon cell adhesion or osseointegration can then be tailored by morphological parameters or surface chemistry. As a consequence, existing treatments of metallic implants can be divided into morphological treatments or surface chemistry modification treatments, the latter being classically subdivided into mineral or organic modification [**45**]. It is worth noting that a commercial solution often uses a combination of the two to maximize cellular response. Of course, impacting morphology of a metallic surface by physical methods leads in the mean time to huge modification of the chemistry of surfaces. Researchers willing to decorrelate the mechanical parameters from the chemical ones have recourse to replicas [**11**, **12**] or nanometer-sized coatings of noble metals (gold, palladium) to control morphology with a unique chemistry [**8**]. Processes

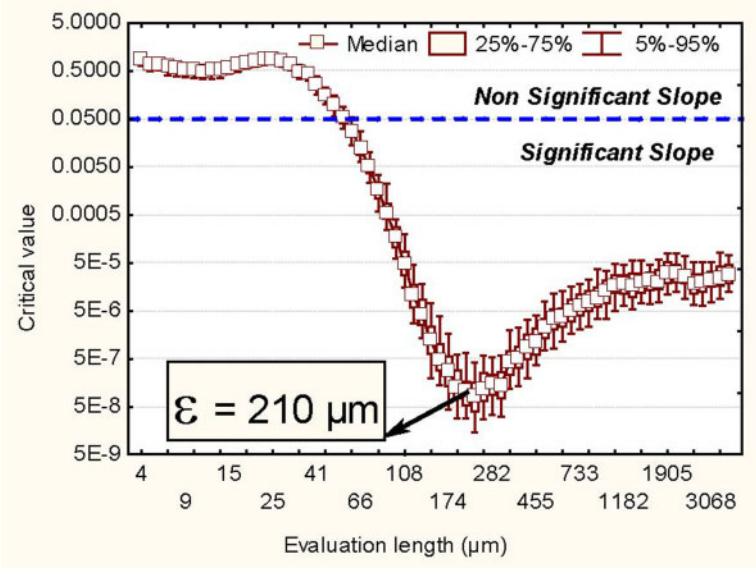

Fig. 8 Bootstrap evolution (100 seeds) of the critical probability that the slope α between contact angle θ and $R_a(\varepsilon)$ parameters is null for the linear relation $\theta(\varepsilon) = \alpha(\varepsilon)\ R_a(\varepsilon) + \beta(\varepsilon)$, as shown in Fig. 8. The lower probability, i.e. that represents the best linear adjustments, is reached at the scale of 210 µm

of surface modification of metallic materials can also be regrouped in physical, chemical, or biochemicals treatments [**46**], the first group being mainly composed of treatments impacting morphology like grit blasting, electro-erosion, plasma treatments, or smoothing; the chemical category includes acidic or alkaline treatments and electrochemical deposition; and finally biochemical treatments are related to conjugation of biological molecules, plasma deposition, or sol–gel coating to mimic biointerfaces. In the present review, it was decided to evaluate the impact on surface chemistry of treatments known to modify the morphology of titanium implants, chemical derivatization to bind biomolecules of interest covalently, and finally, treatments to cover the implant's surface with mineral or organic coatings.

3.1.1 Treatments impacting morphology

Morphological modifications can be induced either by adding a new material that covers the implants (titanium plasma spraying, for example) or removing material from the surface as in the case of grit blasting, chemical etching, or electro-erosion.

Titanium plasma-spraying consists of melting titanium powder in a plasma torch and projecting melted particles on to the surface of the implants. In contact with the surface, the melted particles condense and form a film of several tenths of microns with a roughness R_a parameter of several micrometres [**47**]. This has the advantage of increasing interface area and mechanically strengthening the interface with bone tissue. If treatments are considered that remove material from the surface to change roughness, acidic etching and grit blasting are the most common [**48**]. These treatments increase roughness of the implant to induce a positive response on the bone–implant interface. For grit blasting, aluminium oxide (Al_2O_3), titanium dioxide (TiO_2), or calcium carbonate ($CaCO_3$) particles are projected by a fluid carrier (compressed air or liquid) on to the surface. Such erosion processes have an effect down to the micrometre scale, depending on the size of particles used for blasting, and give surfaces with a R_a index less than 1 µm. Some abrasive particles may be trapped in the final layer, increasing pollution of the sample and modifying the physical–chemical properties of the rough surface. Mechanical abrasion methods will remove the surface oxide layer going down to the metal layer but after cleaning, within seconds, a passivated layer will grow at the surface. The thickness of this native oxide layer is approximately 3–4 nm. The second method used to modify physical parameters of metallic implants, i.e. chemical etching, acts on the dissolution of this native oxide. It can be done in acidic or alkaline condition on titanium, usually with strong acids like HCl, HNO_3, H_2SO_4, H_3PO_4, and even HF. Acidic etching modifies the oxide surface by introducing Ti–OH acidic hydroxyl groups (doubly coordinated by titanium atoms). Alkaline treatment with NaOH increases the density and stabilizes the basic hydroxyl groups (singly coordinated to titanium

atoms) at the surface of the metallic oxide owing to the high pH value. The same effect is reported with hydrogen peroxide treatments (H_2O_2) [**49**]. Basic hydroxide groups seem to favour apatite nucleation and crystallization in bioceramics. This top layer is highly hydrated, giving rise to a layer whose structure is comparable to a hydrogel [**50**]. Titanate species can precipitate and equilibrium between dissolution and hydration creates defects in the oxide layer. Acid etching processes are also known to dissolve alumina particles embedded in the layer after a grit-blasting process. For this reason, the two treatments are often combined. The comparison of the extreme surfaces of polished, sand-blasted, acid-etched, and the combination of the sand-blasting process and acid etching shows that oxides and surface hydroxides ratios are modified by the process. Even if these treatments are mainly devoted to the control of morphology, a change in the surface chemistry cannot be avoided and the wettability and contact angle measurements are strongly affected [**51**].

Electrochemical methods consist of immersing the implant in a solution of electrolytes (acids, ions, or oxidants) and connecting it to a pole of an electrical circuit. Three experimental techniques can be described: anodization, electro-polishing, and electro-erosion. Anodization acts on the growth of the oxide layer up to 40 μm, compared to 3–4 nm of the native oxide layer. Exogenous elements like Ca, Si, S, or P coming from the electrolyte are often embedded in the oxide defects of the layer. The oxide layer grows linearly at a mean rate of approximately 2 nm/V [**52**]. Characteristic interferometric colours are obtained by anodic oxidation and these colours are intrinsically correlated to the thickness of the oxide layer and consequently to the potential applied. When the extreme oxide layer is defect-rich, i.e with oxygen vacancies, the surface is more sensible to hydroxylation (for example, in an autoclaving sterilization process) [**53**]. Depending on the acid concentration and potential applied, the equilibrium between oxide dissolution and growth is displaced and micro- or even nanostructures like granules, dots, or nanotubes with a diameter less than 100 nm can be obtained [**54**]. Electro-polishing induces the dissolution of the amorphous native oxide to give a polycrystalline metallic surface. On this basis, the new oxide layer is devoid of defects, dense, and exhibits a reduced roughness. For the electro-erosion process, the vicinity of a Cu–Zn wire from the surface initiates a plasma zone which locally melts the surface of the titanium implants and grows a TiO_2 layer [**55**]. Contaminations with copper and zinc can also occur [**8**].

3.1.2 Organic chemical modification of implants

Some of the aforementioned treatments cause the extreme surface of implants to be mainly composed of hydroxyl groups. These hydroxyl groups can be used to react a functionalized silane molecule and give self-assembled monolayers (SAMs). Aminopropyl triethoxysilane is one of the common silanes used for chemical derivatization of implants. It is known to give a multi-layer structure with a high density of amino reactive groups. This is the first chemical step to immobilize selected proteins or peptides on to a metallic surface. Immobilizing peptides or proteins on to an implant surface leads to biomimetic surfaces that control or aim to trigger cascading events, occurring when cells reach the surface. To keep the bioactivity of peptides intact, however, the use of a linker that moves the active molecule away from the surface is necessary. For example, glutaraldehyde will react with NH_2 functional groups of the SAMs and with NH_2 groups of the peptide. Maleimide groups are also used as linkers for their property to bind free thiol groups (–SH) of proteins. Other molecules, like growth factors and enzymes, have successfully been conjugated on metallic surfaces. A peptide-like RGD (sequence of arginine, glycine, and aspartic acid residues) covalently bound on to the implant surface mimics fibronectin and causes the cell's receptor to interact directly with the interesting domain of the protein [**56**]. This is a cost-effective solution, avoiding the time-consuming protein purification step. Unfortunately, compared to the entire protein, a single domain like RGD lacks the cooperative influence of other domains of the protein, such as PHSRN for instance, which are known to help the integrin receptor to interact with RGD domains in an appropriate tridimensional localization [**57**]. As can be seen, accessibility and conformation of the peptidic domain of interest are key issues in order to have a bioactive surface for implants. Thus, an immobilization strategy needs to take into account and control the orientation and conformation of the immobilized biomolecule [**58**].

3.1.3 Coatings of implants

The surface chemistry can also be controlled by the deposition of another material with a good adhesion on to the implant. In this case, it is usual to take the benefit of the mechanical properties of the metallic implant and confer interesting functionality via the coating. Such coatings can be realized with organic or mineral layers. Plasma polymerization is one organic coating method that presents good adhesion on a

wide range of substrates [**59**, **60**]. The monomer is flushed into the plasma chamber containing the implant to be coated. Equilibrium between erosion, cleaning, ionization, radical formation, and deposition is formed in the vicinity of the surface and, by adjusting plasma parameters, a thick coating with finely tuned properties can be obtained [**61**]. Acrylic acid monomer gives a final coating of polyacrylic acid with a high density of carboxylic groups [**62**]. As for the SAMs in the previous section, carboxylic groups of the coating can be used to graft protein or peptides after activation with carbodiimides. Mineral coatings made of hydroxyapatite (HAp) are good synthetic candidates to mimic natural bone composition and induce a positive response of cells in orthopaedic implants. Historically, HAp coatings are realized by plasma spraying, owing to its versatility in coating complex shapes of orthopaedic implants [**63–65**]. Sol–gel techniques consist of spin coating an organic precursor of calcium, such as calcium diethoxide. Once the amorphous organic layer has covered the implant surface, a thermal treatment converts the layer into crystallized HAp [**66**]. Unfortunately, experimental conditions are tenuous in order to obtain a single crystalline phase. Usually, a biphasic layer of HAp and calcium oxide is synthesized after thermal treatment [**67**]. HAp can also be coated on titanium surfaces by direct precipitation in simulated body fluid [**68**]. It can be noted that thermally grown oxide seems to favour the precipitation of HAp, whereas oxide surfaces obtained by anodic oxidation limit the deposition [**69**]. The electrolytic deposition method in a solution containing calcium and phosphate ions is another way to obtain biomimetic HAp coatings [**70**].

3.2 Methods of analysis

X-ray diffraction experiments provide information about crystallographic phases present in the sample. This information, depending on the substrate, is relevant at a few micrometres depth. For titanium dioxide, the most stable crystallographic phase is rutile (tetragonal structure). It can only be detected if the oxide thickness is greater than 1 μm. Thus, the native oxide layer, amorphous in nature, with a thickness of several nanometers, is unlikely to be detected by this technique. Polished and acid-etched titanium samples are covered with an amorphous oxide layer as for anodisation in mild conditions. For higher applied voltages, the oxide layer is thicker and crystallizes in an anatase form (tetragonal phase but less closely packed). Thermally grown oxide, on the contrary, crystallizes in a rutile form [**71**].

Surface-sensitive spectrometric techniques such as X-ray photoelectron spectroscopy (XPS) can unravel the structure of the outer chemical layer of the material. The depth of analysis is approximately 8–9 nm depending on the inelastic mean free path of photoelectrons travelling in the outermost layer. In the case of metallic compounds used as screws or structural elements of implants, the surface energy is thermodynamically reduced by formation of a passivating layer of oxide. As an example, titanium $Ti2p_{3/2}$ core line of XPS spectra shows four oxidation states: metallic titanium (Ti(0), 453.8 eV), TiO (Ti(+II), 455.1 eV), Ti_2O_3 (Ti(+III), 456.4 eV), and the outermost TiO_2 (Ti(+IV), 458.5 eV) (Fig. 9). The spin orbit coupling between $Ti2p_{3/2}$ and $Ti2p_{1/2}$ is 5.7 eV [**72–74**] giving eight components overall for the entire Ti2p spectrum ($Ti2p_{3/2}$ and $Ti2p_{1/2}$). The XPS technique is quantitative and, as seen in Fig. 9 for a polished titanium sample, TiO_2 accounts for more than 79 per cent of the titanium total signal. Angle-resolved XPS is able to give hierarchical information over the depth of analysis. Moreover, the non-destructive atomic profile of the layer can be reconstructed by mathematical algorithms. This indicates that titanium dioxide is located at the surface and the sublayer mainly comprises a blend of TiO and Ti_2O_3 phases. The metallic state can be found below these two layers when the two oxide layers do not exceed the probing depth. As the oxide layer still has high surface energy, it will interact with water, polar components, and finally non-polar molecules of the atmosphere. Such thermodynamically driven processes occur in less than 1 s of contact with the

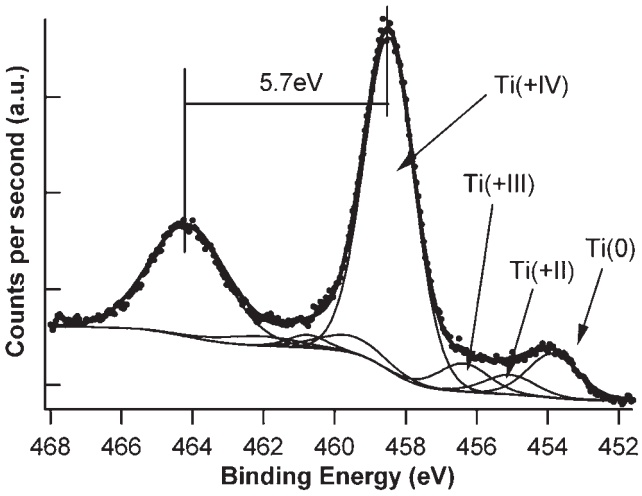

Fig. 9 Ti2p core level spectrum of polished titanium sample. The spin orbit coupling between $Ti2p_{3/2}$ and $Ti2p_{1/2}$ is 5.7 eV and the four-chemical environment of titanium can be detected

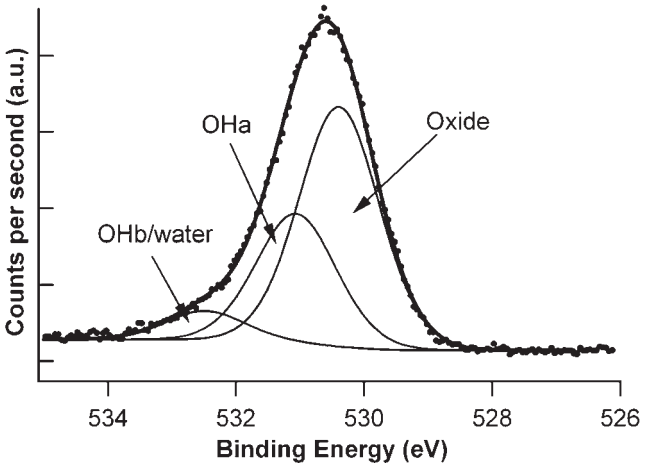

Fig. 10 O1s core level spectrum of polished titanium cleaned by argon plasma for a duration of 2 min. Curve fitting reveals oxides, acidic hydroxides (OH_a), and basic hydroxides/water components (OH_b)

atmosphere. This is why a common implant surface can exhibit an amount of carbon of the order of 40 per cent, and even 75 per cent, if no care is taken during the manipulation and storage of implants. In particular, oils and detergents of machining tools are one of the major sources of carbonaceous pollution of implants. The XPS O1s core level spectrum is helpful to consider the hydroxides or water layer present at the surface of titanium implants after mechanical treatment. The core level O1s spectrum of polished titanium is depicted in Fig. 10. It can be curve-fitted with three components: the first is related to oxides at a binding energy of 530.3 eV, the second reflects the chemical environment of acidic hydroxide (OH_a) at 531.1 eV, and the last component appears at 532.5 eV for basic hydroxides or water adsorbed (OH_b). It can be noted that the amount of hydroxides present on the surface is strongly dependent on the hydration state of the implant, as well as ageing. In particular, as it has been shown for monolayers, sterilization processes like autoclaving or dry heat are likely to alter the hydroxide surface composition [**75**]. The determination of surface chemistry, and in particular the ratio of oxide/hydroxide, is intrinsically linked to the wettability behaviour of the implants. Determination of contact angle and surface free energy is a simple way to assess hydrophilicity of implants. Numerous articles in the literature deal with the relation between hydrophilicity and performance of implants [**48**, **51**, **76**–**78**].

As most morphological assessments are realized with the help of SEM, the surface composition of implants is also often determined by energy dispersive X-ray analysis (EDX). In this case, the probing depth can be higher than several microns and comparison with XPS results remains difficult [**79**].

Time-of-flight secondary ions mass spectroscopy (ToF SIMS) is able to give information about the metallic surface of implants [**80**, **81**]. It can also be a forensic tool for protein fouling when implants are immersed in a biological medium [**82**] or, by using suitable mass fragments, can follow the growth of a mineral layer or bone regeneration [**83**, **84**]. As for XPS, this technique has the restriction that it must be operated in an ultra high vacuum and so cannot be used *in situ*. The main advantage remains in its extreme surface sensitivity, which makes it suitable to monitor tenuous changes in the surface chemistry.

As well as morphological treatments that modify surface chemistry of implants, morphological parameters such as roughness impact the signal of XPS, ToF SIMS, or other physical techniques of characterization. Some attempts have been made to take into account a geometrical roughness and evaluate the impact on the XPS signal [**85**, **86**]. Nevertheless, the level of complexity of roughness parameters described in the first part of this article is far from being achieved.

This illustrates once more the difficulty of probing, in the mean time, the chemistry and topography or morphology of real implants at a significant scale for cell adhesion. The biological relevance of these parameters will be assessed in the second part of this review.

4 CONCLUSION

Knowledge of the complexity of the cell–material interactions is essential for the future of biomaterials and tissue engineering, but we are still far from achieving a clear understanding, as illustrated in this review. Many factors on the cellular or the material side influence these interactions and must be controlled systematically during experiments. On the material side, the necessity to illustrate surface topography by parameters describing the roughness amplitude, as well as the roughness organization, and at all scales pertinent to the cell response (i.e. from the nanoscale to the micro-scale) has been underlined. Researchers interested in this field must be careful to develop systematically surfaces or methods allowing perfect control of the relative influences of surface topography and surface chemistry. Finally, understanding of the role of surface physico-chemistry in protein adsorption is also an exciting task for the future, considering the limited control and

knowledge currently available experimentally regarding the protein adsorption on implant materials and considering the crucial importance that proteins have in cell response to materials. This is the 'black box' of the field and elucidation of the rules underlying protein adsorption on implant surfaces would certainly allow control of the cellular interactions with implant materials.

REFERENCES

1 **Boyan, B. D., Hummert, T. W., Dean, D. D.,** and **Schwartz, Z.** Role of material surfaces in regulating bone and cartilage cell response. *Biomaterials*, 1996, **17**, 137–146.

2 **Brunette, D. M.** and **Chehroudi, B.** The effects of the surface topography of micromachined titanium substrata on cell behavior in vitro and in vivo. *J. Biomech. Engng*, 1999, **121**, 49–57.

3 **Anselme, K.** Osteoblast adhesion on biomaterials. *Biomaterials*, 2000, **21**, 667–681.

4 **Boyan, B. D., Lohmann, C. H., Dean, D. D., Cochran, D. L.,** and **Schwartz, Z.** Mechanisms involved in osteoblast response to implant surface morphology. *Annual Rev. Mater. Res.*, 2001, **31**, 357–371.

5 **Dalby, M. J.** Topographically induced direct cell mechanotransduction. *Med. Engng Physics*, 2005, **27**, 730–742.

6 **Meyer, U., Büchter, A., Wiesmann, H. P., Joos, U.,** and **Jones, D. B.** Basic reactions of osteoblasts on structured material surfaces. *Eur. Cells Mater.*, 2005, **9**, 39–49.

7 **Hacking, S. A., Tanzer, M., Harvey, E. J., Krygier, J. J.,** and **Bobyn, J. D.** Relative contributions of chemistry and topography to the osseointegration of hydroxyapatite coatings. *Clin. Orthop. Related Res.*, 2002, **405**, 24–38.

8 **Anselme, K.** and **Bigerelle, M.** Effect of a gold–palladium coating on the long-term adhesion of human osteoblasts on biocompatible metallic materials. *Surf. Coating Technol.*, 2006, **200**, 6325–6330.

9 **Anselme, K.** and **Bigerelle, M.** Statistical demonstration of the relative effect of surface chemistry and roughness on human osteoblast short-term adhesion. *J. Mater. Sci. – Mater. Medicine*, 2006, **17**, 471–479.

10 **dos Santos, E. A., Farina, M., Soares, G. A.,** and **Anselme, K.** Chemical and topographical influence of hydroxyapatite and beta-tricalcium phosphate surfaces on human osteoblastic cell behavior. *J. Biomed. Mater. Res. A*, 2009, **89**, 510–520.

11 **Wieland, M., Chehroudi, B., Textor, M.,** and **Brunette, D. M.** Use of Ti-coated replicas to investigate the effects on fibroblast shape of surfaces with varying roughness and constant chemical composition. *J. Biomed. Mater. Res.*, 2002, **60**, 434–444.

12 **Schuler, M., Kunzler, T. P., de Wild, M., Sprecher, C. M., Trentin, D., Brunette, D. M., Textor, M.,** and **Tosatti, S. G.** Fabrication of TiO_2-coated epoxy replicas with identical dual-type surface topographies used in cell culture assays. *J. Biomed. Mater. Res. A*, 2009, **88**, 12–22.

13 **Anselme, K.** and **Bigerelle, M.** Topography effects of pure titanium substrates on human osteoblast long-term adhesion. *Acta Biomater.*, 2005, **1**, 211–222.

14 **Gautier, A., Revel, P., Mazeran, P. E.,** and **Bigerelle, M.** The relevance of topographic measurements on high precision machined surfaces. *Materiaux et Techniques*, 2007, **95**, 37–46.

15 **Poon, C. Y.** and **Bhushan, B.** Comparison of surface roughness measurements by stylus profiler, AFM and non-contact optical profiler. *Wear*, 1995, **190**, 76–88.

16 **Jouini, N., Gautier, A., Revel, P., Mazeran, P. E.,** and **Bigerelle, M.** Multi-scale analysis of high precision surfaces by stylus profiler, scanning white-light interferometry and atomic force microscopy. *Int. J. Surf. Sci. Engng*, 2009, **3**, 310–327.

17 **Eaton, P.** and **West, P.** *Atomic force microscopy*, 2010 (Oxford University Press, Oxford).

18 **Leang, K. K.** and **Devasia, S.** Design of hysteresis-compensating iterative learning control for piezo-positioners: Application to atomic force microscopes. *Mechatronics*, 2006, **16**, 141–158.

19 **Mazeran, P. E., Odoni, L.,** and **Loubet, J. L.** Curvature radius analysis for scanning probe microscopy. *Surf. Sci.*, 2005, **585**, 25–37.

20 **Snaith, B., Edmondst, M. J.,** and **Probert, S. D.** Use of a profilometer for surface mapping. *Precis Eng*, 1981, **3**, 87–90.

21 **Bigerelle, M., Gautier, A., Hagege, B., Favergeon, J.,** and **Bounichane, B.** Roughness characteristic length scales of belt finished surface. *J. Mater. Processing Technol.*, 2009, **209**, 6103–6116.

22 **Bigerelle, M., Gautier, A.,** and **Iost, A.** Roughness characteristic length scales of micro-machined surfaces: A multi-scale modelling. *Sensors Actuators B – Chemistry*, 2007, **126**, 126–137.

23 **Pawlus, P.** and **Smieszek, M.** The influence of stylus flight on change of surface topography parameters. *Precision Engng – J. Int. Soc. Precision Engng Nanotechnol.*, 2005, **29**, 272–280.

24 **Lockwood, D. J.** *Light scattering and nanoscale surface roughness*, in Nanostructure Science and Technology, (Ed. A.A. Maraduden), Springer (New York), 2007.

25 **Najjar, D., Bigerelle, M., Migaud, H.,** and **Iost, A.** Identification of scratch mechanisms on a retrieved metallic femoral head. *Wear*, 2005, **258**, 240–250.

26 **Najjar, D., Bigerelle, M., Migaud, H.,** and **Iost, A.** About the relevance of roughness parameters used for characterizing worn femoral heads. *Tribology Int.*, 2006, **39**, 1527–1537.

27 **Bigerelle, M.** and **Iost, A.** A numerical method to calculate the Abbott parameters: A wear application. *Tribology Int.*, 2007, **40**, 1319–1334.

28 **Bigerelle, M.** and **Iost, A.** Calcul de la dimension fractale d'un profil par la méthode des autocorrélations moyennées normées A.M.N. *CR Acad. Sci. Paris*, 1996, **323**, 669–675.

29 **Van Gorp, A., Bigerelle, M., Grellier, A., Iost, A.,** and **Najjar, D.** A multi-scale approach of roughness measurements: Evaluation of the relevant scale. *Mater. Sci. Engng C – Bio S*, 2007, **27**, 1434–1438.

30 **Whitehouse, D. J.** *Handbook of surface metrology*, 1994 (Institute of Physics).

31 **Stout, K. J., Sullivan, P. J., Dong, W. P., Mainsah, E., Luo, N., Mathia, T.,** and **Zahouani, H.** *Development of methods for the characterization of roughness in three dimensions*, 2000 (Penton Press, London).

32 **International Organization for Standardization**. ISO 1302: Geometrical product specification (GPS) – indication of surface texture in technical product documentation, 2002 (ISO, Geneva).

33 **American Society for Mechanical Engineers**. ASME Y14.36M: Surface texture symbols, 1996 (ASME, New York).

34 **International Organization for Standardization**. ISO1302: Geometrical product specification (GPS) – indication of surface texture in technical product documentation, 2005 (ISO, Geneva).

35 **Bigerelle, M.** and **Iost, A.** A numerical method to calculate the Abbott parameters: A wear application. *Tribology Int.*, 2007, **40**, 1319–1334.

36 **Bigerelle, M., Najjar, D.,** and **Iost, A.** Multiscale functional analysis of wear – A fractal model of the grinding process. *Wear*, 2005, **258**, 232–239.

37 **Bigerelle, M., Van Gorp, A., Gautier, A.,** and **Revel, P.** Multiscale morphology of high-precision turning process surfaces. *Proc. IMechE, Part B: J. Engineering Manufacture*, 2007, **221**, 1485–1497. DOI: 10.1243/09544054JEM777.

38 **Bigerelle, M., Van Gorp, A.,** and **Lost, A.** Multiscale roughness analysis in injection-molding process. *Polymer Engng Sci.*, 2008, **48**, 1725–1736.

39 **Van Gorp, A., Bigerelle, M., El Mansori, M., Ghidossi, P.,** and **Iost, A.** Effects of working parameters on the surface roughness in belt grinding process: the size–scale estimation influence. *Int. J. Mater. Prod. Technol.*, 2010, **38**, 16–34.

40 **Bigerelle, M., Najjar, D.,** and **Iost, A.** Relevance of roughness parameters for describing and modelling machined surfaces. *J. Mater. Sci.*, 2003, **38**, 2525–2536.

41 **Najjar, D., Bigerelle, M.,** and **Iost, A.** The computer-based bootstrap method as a tool to select a relevant surface roughness parameter. *Wear*, 2003, **254**, 450–460.

42 **Hennebelle, F., Najjar, D., Bigerelle, M.,** and **Iost, A.** Influence of the morphological texture on the low wear damage of paint coated sheets. *Prog. Org. Coatings*, 2006, **56**, 81–89.

43 **Najjar, D., Bigerelle, M., Hennebelle, F.,** and **Iost, A.** Contribution of statistical methods to the study of worn paint coatings surface topography. *Surf. Coating Technol.*, 2006, **200**, 6088–6100.

44 **Giljean, S., Najjar, D., Bigerelle, M.,** and **Iost, A.** Multiscale analysis of abrasion damage on stainless steel. *Surf. Engng*, 2008, **24**, 8–17.

45 **Schliephake, H.** and **Scharnweber, D.** Chemical and biological functionalization of titanium for dental implants. *J. Mater. Chemistry*, 2008, **18**, 2404–2414.

46 **Puleo, D. A.** and **Nanci, A.** Understanding and controlling the bone–implant interface. *Biomaterials*, 1999, **20**, 2311–2321.

47 **Le Guehennec, L., Soueidan, A., Layrolle, P.,** and **Amouriq, Y.** Surface treatments of titanium dental implants for rapid osseointegration. *Dent. Mater.*, 2007, **23**, 844–854.

48 **Ferguson, S. J., Broggini, N., Wieland, M., de Wild, M., Rupp, F., Geis-Gerstorfer, J., Cochran, D. L.,** and **Buser, D.** Biomechanical evaluation of the interfacial strength of a chemically modified sandblasted and acid-etched titanium surface. *J. Biomed. Mater. Res. A*, 2006, **78**, 291–297.

49 **Ohtsuki, C., Iida, H., Hayakawa, S.,** and **Osaka, A.** Bioactivity of titanium treated with hydrogen peroxide solutions containing metal chlorides. *J. Biomed. Mater. Res.*, 1997, **35**, 39–47.

50 **Bagno, A.** and **Di Bello, C.** Surface treatments and roughness properties of Ti-based biomaterials. *J Mater Sci-Mater Med*, 2004, **15**, 935–949.

51 **Rupp, F., Scheideler, L., Olshanska, N., de Wild, M., Wieland, M.,** and **Geis-Gerstorfer, J.** Enhancing surface free energy and hydrophilicity through chemical modification of microstructured titanium implant surfaces. *J. Biomed. Mater. Res. A*, 2006, **76**, 323–334.

52 **Sul, Y. T., Johansson, C. B., Jeong, Y.,** and **Albrektsson, T.** The electrochemical oxide growth behaviour on titanium in acid and alkaline electrolytes. *Med. Engng Physics*, 2001, **23**, 329–346.

53 **Lausmaa, J.** Surface spectroscopic characterization of titanium implant materials. *J. Electron Spectroscopy*, 1996, **81**, 343–361.

54 **Kim, S. E., Lim, J. H., Lee, S. C., Nam, S. C., Kang, H. G.,** and **Choi, J.** Anodically nanostructured titanium oxides for implant applications. *Electrochimica Acta*, 2008, **53**, 4846–4851.

55 **Bigerelle, M., Anselme, K., Noël, B., Ruderman, I., Hardouin, P.,** and **Iost, A.** Improvement in the morphology of surfaces for cell adhesion: a new process to double human osteoblast adhesion on Ti-based substrates. *Biomaterials*, 2002, **23**, 1563–1577.

56 **Schliephake, H., Scharnweber, D., Dard, M., Sewing, A., Aref, A.,** and **Roessler, S.** Functionalization of dental implant surfaces using adhesion molecules. *J. Biomed. Mater. Res. B*, 2005, **73**, 88–96.

57 **Keselowsky, B. G.** and **Garcia, A. J.** Quantitative methods for analysis of integrin binding and focal adhesion formation on biomaterial surfaces. *Biomaterials*, 2005, **26**, 413–418.

58 **Rezania, A.** and **Healy, K. E.** The effect of peptide surface density on mineralization of a matrix deposited by osteogenic cells. *J. Biomed. Mater. Res.*, 2000, **52**, 595–600.

59 **Puleo, D. A., Kissling, R. A.,** and **Sheu, M. S.** A technique to immobilize bioactive proteins, including bone morphogenetic protein-4 (BMP-4), on titanium alloy. *Biomaterials*, 2002, **23**, 2079–2087.

60 **Hayakawa, T., Yoshinari, M.,** and **Nemoto, K.** Characterization and protein-adsorption behavior of deposited organic thin film onto titanium by plasma polymerization with hexamethyldisiloxane. *Biomaterials*, 2004, **25**, 119–127.

61 **Ploux, L., Anselme, K., Dirani, A., Ponche, A., Soppera, O.,** and **Roucoules, V.** Opposite responses of cells and bacteria to micro/nanopatterned surfaces prepared by pulsed plasma polymerization and UV-irradiation. *Langmuir*, 2009, **25**, 8161–8169.

62 **Morra, M., Cassinelli, C., Cascardo, G., Cahalan, P., Cahalan, L., Fini, M.,** and **Giardino, R.** Surface engineering of titanium by collagen immobilization. Surface characterization and in vitro and in vivo studies. *Biomaterials*, 2003, **24**, 4639–4654.

63 **Chu, P. K.** Applications of plasma-based technology to microelectronics and biomedical engineering. *Surf. Coating Technol.*, 2009, **203**, 2793–2798.

64 **Zheng, X. B., Huang, M. H.,** and **Ding, C. X.** Bond strength of plasma-sprayed hydroxyapatite/Ti composite coatings. *Biomaterials*, 2000, **21**, 841–849.

65 **Yang, Y. Z.** and **Ong, J. L.** Bond strength, compositional, and structural properties of hydroxyapatite coating on Ti, ZrO2-coated Ti, and TPS-coated Ti substrate. *J. Biomed. Mater. Res. A*, 2003, **64**, 509–516.

66 **Zreiqat, H., Valenzuela, S. M., Nissan, B. B., Roest, R., Knabe, C., Radlanski, R. J., Renz, H.,** and **Evans, P. J.** The effect of surface chemistry modification of titanium alloy on signalling pathways in human osteoblasts. *Biomaterials*, 2005, **26**, 7579–7586.

67 **Milev, A. S., Kannangara, G. S. K., Ben-Nissan, B.,** and **Wilson, M. A.** Temperature effects on a hydroxyapatite precursor solution. *J. Phys Chem.; B*, 2004, **108**, 5516–5521.

68 **Yang, B. C., Uchida, M., Kim, H. M., Zhang, X. D.,** and **Kokubo, T.** Preparation of bioactive titanium metal via anodic oxidation treatment. *Biomaterials*, 2004, **25**, 1003–1010.

69 **Wang, X. X., Yan, W., Hayakawa, S., Tsuru, K.,** and **Osaka, A.** Apatite deposition on thermally and anodically oxidized titanium surfaces in a simulated body fluid. *Biomaterials*, 2003, **24**, 4631–4637.

70 **Duan, K.** and **Wang, R. Z.** Surface modifications of bone implants through wet chemistry. *J. Mater. Chemistry*, 2006, **16**, 2309–2321.

71 **Birch, J. R.** and **Burleigh, T. D.** Oxides formed on titanium by polishing, etching, anodizing, or thermal oxidizing. *Corrosion*, 2000, **56**, 1233–1241.

72 **Marino, C. E. B., Nascente, P. A. P., Biaggio, S. R., Rocha, R. C.,** and **Bocchi, N.** XPS characterization of anodic titanium oxide films grown in phosphate buffer solutions. *Thin Solid Films*, 2004, **468**, 109–112.

73 **Godfroid, T., Gouttebaron, R., Dauchot, J. P., Leclere, P., Lazzaroni, R.,** and **Hecq, M.** Growth of ultrathin Ti films deposited on SnO2 by magnetron sputtering. *Thin Solid Films*, 2003, **437**, 57–62.

74 **Sul, Y.-T., Johansson, C. B., Petronis, S., Krozer, A., Jeong, Y., Wennerberg, A.,** and **Albrektsson, T.** Characteristics of the surface oxides on turned and electrochemically oxidized pure titanium implants up to dielectric breakdown: the oxide thickness, micropore configurations, surface roughness, crystal structure and chemical composition. *Biomaterials*, 2002, **23**, 491–501.

75 **Fleith, S., Ponche, A., Bareille, R., Amedee, J.,** and **Nardin, M.** Effect of several sterilisation techniques on homogeneous self assembled monolayers. *Colloid Surf. B*, 2005, **44**, 15–24.

76 **Taborelli, M., Jobin, M., François, P., Vaudaux, P., Tonetti, M., Szmukler-Moncler, S., Simpson, J. P.,** and **Descouts, P.** Influence of surface treatments developed for oral implants on the physical and biological properties of titanium. (I) Surface characterization. *Clin. Oral Implant Res.*, 1997, **8**, 208–216.

77 **Ponsonnet, L., Reybier, K., Jaffrezic, N., Comte, V., Lagneau, C., Lissac, M.,** and **Martelet, C.** Relationship between surface properties (roughness, wettability) of titanium and titanium alloys and cell behaviour. *Mater. Sci. Engng C*, 2003, **23**, 551–560.

78 **Kilpadi, D. V.** and **Lemons, J. E.** Surface-energy characterization of unalloyed titanium implants. *J. Biomed. Mater. Res.*, 1994, **28**, 1419–1425.

79 **Kang, B. S., Sul, Y. T., Oh, S. J., Lee, H. J.,** and **Albrektsson, T.** XPS, AES and SEM analysis of recent dental implants. *Acta Biomater.*, 2009, **5**, 2222–2229.

80 **Lu, X., Wang, Y., Yang, X., Zhang, Q., Zhao, Z., Weng, L. T.,** and **Leng, Y.** Spectroscopic analysis of titanium surface functional groups under various surface modification and their behaviors in vitro and in vivo. *J. Biomed. Mater. Res.*, 2008, **84**, 523–534.

81 **Petersson, I. U., Loberg, J. E. L., Fredriksson, A. S.,** and **Ahlberg, E. K.** Semi-conducting properties of titanium dioxide surfaces on titanium implants. *Biomaterials*, 2009, **30**, 4471–4479.

82 **Cacciafesta, P., Hallam, K. R., Watkinson, A. C., Allen, G. C., Miles, M. J.,** and **Jandt, K. D.** Visualisation of human plasma fibrinogen adsorbed on titanium implant surfaces with different roughness. *Surf. Sci.*, 2001, **491**, 405–420.

83 **Coelho, P. G.** and **Lemons, J. E.** Physico/chemical characterization and in vivo evaluation of nanothickness bioceramic depositions on alumina-blasted/acid-etched Ti-6Al-4V implant surfaces. *J. Biomed. Mater. Res. A*, 2009, **90A**, 351–361.

84 **Eriksson, C., Borner, K., Nygren, H., Ohlson, K., Bexell, U., Billerdahl, N.,** and **Johansson, M.** Studies by imaging TOF–SIMS of bone mineralization on porous titanium implants after 1 week in bone. *Appl. Surf. Sci.*, 2006, **252**, 6757–6760.

85 **De Bernardez, L. S., Ferron, J., Goldberg, E. C.,** and **Buitrago, R. H.** The effect of roughness on XPS and AES. *Surf. Sci.*, 1984, **139**, 541–548.

86 **Gunter, P. L. J., Gijzeman, O. L. J.,** and **Niemantsverdriet, J. W.** Surface roughness effects in quantitative XPS: magic angle for determining overlayer thickness. *Appl. Surf. Sci.*, 1997, **115**, 342–346.